Chemistry and rotational excitation of O_2 in interstellar clouds

I. Predicted emissivities of lines for the ODIN, SWAS, PRONAOS-SMH and PIROG 8 submillimeter receivers

P. Maréchal[1]**, Y.P. Viala**[1]**, and J.J. Benayoun**[2]

[1] Observatoire de Paris, DEMIRM, URA 336 du CNRS, 61 Av. de l'Observatoire, F-75014 Paris, France
[2] Observatoire de Grenoble, Laboratoire d'Astrophysique, Université Joseph Fourier, B.P.53X, F-38041 Grenoble Cedex, France

Abstract. Molecular oxygen has not yet been observed in interstellar clouds because of the opacity of the Earth's atmosphere. Due to its potential importance in interstellar chemistry, several projets attempting to detect rotational lines of O_2 are being developed using millimeter and submillimeter receivers embarked on satellites or stratospheric balloons: ODIN for the 119 and 487 GHz lines, SWAS for the 487 GHz line, PRONAOS-SMH for the 368 GHz line and PIROG 8 for the 425 GHz line. As a theoretical preparation to these projects and taking advantage of recent developments in interstellar chemistry as well as recent cross-section calculations of collisional excitation of O_2, we have used an interstellar cloud model to perform a non-LTE calculation of O_2 rotational population. O_2 column densities and emissivities of its rotational lines at (sub)millimeter wavelengths are predicted for various conditions in diffuse, translucent and dense dark clouds, covering a range of visual extinction from 1 to 30. The effects of density, temperature, external ultraviolet radiation field and gas phase elemental abundances on the O_2 abundance and rotational excitation have been investigated. Our results are confronted to the ones obtained by Black & Smith (1984) who adressed initially the problem of the detectability of interstellar O_2. If density and temperature have little influence on the O_2 abundance, it is not the case for the UV radiation field which efficiently destroys O_2 so as to prevent its detection in most clouds as soon as it is enhanced by a factor of 1000 with respect to the local standard value. The most drastic parameter that influences the abundance of O_2 — as well as that of OH and H_2O — is the gas-phase C/O abundance ratio: for C/O ratio larger than 0.7, O_2 becomes unobservable by all forthcoming missions except for the 119 GHz line which remains observable in very opaque clouds ($A_V \sim 20$) up to C/O = 1. The rate coefficient of the reaction $O+OH \rightarrow O_2+H$ which produces molecular oxygen has little influence on the O_2 abundance in clouds sufficiently opaque to allow detection; it however controls the OH abundance since it is the main destruction process of this molecule. Our model calculations also predict that the radiative de-excitation of O_2 rotational levels could be an important cooling agent in cold molecular clouds with an efficiency comparable to that of CO.

1. Introduction

Because of the large cosmic abundance of oxygen, this element plays a major role in the chemistry of interstellar molecular clouds. Much theoretical work has been devoted to the synthesis of oxygen-bearing molecules. At the same time, around 30 molecules containing oxygen, representing nearly half of the molecules so far detected in space, have now been observed in interstellar and circumstellar environments. Many of these oxygen-bearing species are only trace compounds with very low abundances but some of them are among the most complex organic molecules observed, revealing the surprisingly richness of interstellar chemistry. The most abundant and famous oxygen-bearing molecule is CO which is observed in a large variety of physical conditions and used as a tracer of molecular gas in galaxies. Chemical models of interstellar clouds, beginning with the first ones dealing with steady-state abundance calculations of the simplest molecules (Herbst & Klemperer 1973, Viala & Walmsley 1976) predict that molecular oxygen O_2 has an abundance comparable to that of CO deep inside molecular clouds and plays an important role for controlling the abundance of other molecules. This has been confirmed by further chemical models, at least by those assuming steady-state equilibrium.

For these reasons, observation of molecular oxygen and measurement of its abundance could permit to test the interstellar chemistry and to give some insight on the total amount of oxygen in the gas phase of molecular clouds. Despite the presumed importance of O_2 in the interstellar clouds, this molecule

has not yet been observed. The presence of a large quantity of molecular oxygen in the terrestrial atmosphere is a major obstacle to the detection of interstellar O$_2$ by ground-based telescopes. Its observation requires the use of receivers embarked on balloons or satellites and four experiments are in course of development to detect rotational lines within the ground vibrational level. Our laboratory is involved in two of these experiments for which we are developing two submillimeter heterodyne supraconducting (SIS) receivers. The first one will be borne by the stratospheric balloon-borne observatory PRONAOS-SMH developed under the responsability of the CNES to search for the (N, J): $(3, 2) \rightarrow (1, 1)$ line of O$_2$ at 368 GHz (Beaudin et al. 1994). The second one will equip the swedish-french balloon PIROG 8 to search for the $(3, 2) \rightarrow (1, 2)$ line at 425 GHz. Two other projects are: the US satellite SWAS which will observe the $(3, 3) \rightarrow (1, 2)$ line at 487 GHz and the swedish satellite ODIN, developed with the collaboration of Canada, France and Finland devoted to a search for both the 119 GHz and 487 GHz lines.

The main purpose of this paper is to make theoretical predictions of the emissivities of these O$_2$ lines and of some others. To do this, radiative and collisional transfers between the rotational levels of O$_2$ have been included in a model which calculates chemical and thermal balance in molecular clouds. Modelling the chemistry and rotational excitation of molecular oxygen previously done by Black & Smith (1984). New data about chemical and collisional processes led us to adress this problem again and to make a more extensive study of the influence of several physical parameters on the abundance and rotational excitation of O$_2$. The model is presented in Sect. 2 including the determination of the spectroscopic parameters of O$_2$ in its ground vibrational level which are needed to compute its rotational population. Several parameters could affect the abundance and the emissivity of O$_2$ such as total visual extinction, temperature, density, ultraviolet radiation field or C/O elemental abundance ratio. The influence of these parameters are discussed in Sect. 3. The effects of radiative cooling due to O$_2$ have been accurately estimated and are presented in the same section. Sect. 4 summarizes our main conclusions.

2. The cloud model. Chemistry and rotational excitation of O$_2$

2.1. The steady-state model

The model of molecular cloud used here is described in a detailed way in Warin et al. (1996). It calculates chemical and thermal balance by assuming steady-state equilibrium. It only applies to quiescent interstellar molecular clouds, excluding shocks and photodissociation regions. It takes into account variations of physical parameters with position within the cloud, and particularly, the variations due to the attenuation of the ultraviolet radiation field as it penetrates into the cloud. The abundances of chemical species and the temperature profile throughout the cloud are obtained by solving, in a self-consistent way, the radiative transfer equation for ultraviolet photons (assuming plane

parallel geometry and absorption by gas and dust), the chemical balance equations and the thermal balance equation. The fine structure excitation of C, C$^+$ and O and the rotational excitation of H$_2$, CO and its isotopes are also treated by solving the statistical equations governing the population of the levels. For our purpose, we have included the rotational excitation of O$_2$ and ^{16}O^{18}O. All processes susceptible to play a role in fine structure or rotational excitation have been taken into account: chemical processes, selective photodissociation of rotational levels (for CO), UV pumping through excited electronic states (for H$_2$), collisional excitation and de-excitation and radiative processes, i.e. absorption, spontaneous and stimulated emission of rotational transitions. Concerning radiative processes, the possibility that photons can be trapped within the medium when the optical depths of the transitions between levels become large is allowed for by the model. The chemical reaction scheme involves 111 chemical species formed from C- and O- bearing species and their ^{13}C and ^{18}O isotopic substitutions and about 2,100 reactions. The heating of the cloud is due to cosmic ray, H$_2$ formation on grains and collisions between gas and dust in the core of the cloud. Photo-destruction, photo-electric effect on dust, dissociation of H$_2$ and ionisation of Mg, Fe, Si, S and C are efficient heating processes at the edge of the cloud. The cooling is due to collisional excitation followed to radiative de-excitation. At the edge of the cloud, the de-excitation of the fine structure levels of C$^+$, C and O is efficient; in the inner parts, the de-excitation of rotational levels of CO, ^{13}CO, C^{18}O is dominant. In some cases and as discussed in Sect. 3.4, cooling by O$_2$ rotational lines can become efficient.

2.2. The chemistry of O$_2$

As previous chemical models have shown, O$_2$ is mainly produced through the neutral-neutral reaction (1):

$$O + OH \rightarrow O_2 + H \tag{1}$$

This reaction has been studied experimentally at room temperature and above, in the range 250–515 K (Howard & Smith 1980); it has a rate coefficient $k_1=(3.8\pm0.9)\ 10^{-11}$ cm^{-3}s^{-1} at 298 K and does not show any activation barrier in this temperature range. To our knowledge, no measurements exist at lower temperature. We adopt here the rate derived by Davidsson & Stenholm (1990) from theoretical calculations (extended Langevin model and quasi classical trajectory method): $k_1=3.3\ 10^{-10}$T$^{-0.4}$exp(-6.0/T) cm^{3}s^{-1} which applies in a range 10–300 K, more appropriate for interstellar cloud modelling. The theoretical rate coefficient is in fair agreement with the measured value at room temperature but is somewhat higher in the range 10–50 K than the value recommended in the UMIST database (Millar et al. 1996).

Photoionisation and photodissociation by UV photons are very efficient destruction processes of the oxygen molecule. From 912 Å, the cut-off of the interstellar radiation field, to 1027 Å, the photoionisation threshold of O$_2$, the molecule can be either ionised or dissociated and both processes occur through

Table 1. Spectroscopic constants for the ground vibrational level of O_2

	MHz
B	43,100.460
D	0.14501
λ_0	59,501.341
λ_1	0.05848
γ_0	-252.586
γ_1	-0.000247

Table 2. Line strengths of O_2 $(N+2, N+1) \rightarrow (N, N)$ calculated from Eqs. (60) and (61) of Tinkham & Strandberg (1955)

N	S_{ul}	N	S_{ul}
1	0.04801	9	0.02035
3	0.03965	11	0.01742
5	0.03044	13	0.01522
7	0.02443	15	0.01352

broad and well-separated peaks; the photoabsorption cross-sections and the ionisation and dissociation yields have been taken from Kirby et al. (1979). From 1250 to 1770 Å, O_2 is dissociated through absorption of photons in the Schumann-Runge $(X^3\Sigma^- \rightarrow B^3\Sigma^-)$ continuum; cross-sections come from Hudson (1971). Absorption of photons in the range 1750–2000 Å, in the Schumann-Runge bands, can also dissociate O_2 since many excited ro-vibrational levels of the $B^3\Sigma^-$ electronic state are pre-dissociated (Gies et al. 1981, Yoshino et al. 1983, Cheung et al. 1993). The contribution to the overall photodissociation rate of O_2 is however negligible due to the combined effect of low absorption oscillator strengths and decrease of the interstellar UV radiation field in this wavelength range. In regions where UV photons are excluded, O_2 is mainly destroyed by reactive collisions with C^+, H^+ and He^+. The library of chemical reactions is extracted from Viala (1986) where only C and O compounds have been kept; rate coefficients have been up-dated according to the compilations by Anicich (1993) for ion-neutral reactions and by Millar et al. (1996) for neutral-neutral reactions.

2.3. The rotational excitation of O_2

To obtain the rotational population of O_2, we take into account the following processes: spontaneous emission, stimulated emission and absorption of the ambient background radiation, collisional excitation and de-excitation. We consider such processes between the first 24 rotational levels of O_2 ($E_{max} \sim 500$ K).

In the radiative terms of the statistical equilibrium (absorption and stimulated emission), the intensity within each line connecting two levels is computed along the way described in Warin et al. (1996) by adopted the escape probability approximation for a plane-parallel cloud of finite thickness.

2.3.1. Energies, frequencies and Einstein coefficients

The ground electronic state of O_2 is a $^3\Sigma$ state with two unpaired electrons. Consequently its rotational levels are split into a spin triplet corresponding to the three possible space orientations of the electronic spin vector **S** . **N** designates the molecular rotational momentum and **J=N+S** , the resulting angular momentum. Since S=1, the possible values of J are $N+1$, N, $N-1$. O_2 consists of two identical atoms obeying to the Bose-Einstein statistics so that levels with even values of N do not occur (Herzberg 1950). Rotational energy levels are obtained from Gordy & Cook (1984) after correcting a misprint in the expression of a:

$$\begin{aligned}
E(N = J, J) &= b \\
E(N = J \pm 1, J) &= \tfrac{1}{2}(a + c) \pm \tfrac{1}{2}\left[(a - c)^2 + 4d^2\right]^{1/2} \\
E(N = J \pm 1, J) &= 2(B - 2D) - 2(\gamma_0 + 2\gamma_1) - \\
&\quad \tfrac{4}{3}(\lambda_0 + 2\lambda_1)
\end{aligned} \quad (2)$$

with

$$\begin{aligned}
a &= BJ(J - 1) - DJ^2(J - 1)^2 + \gamma_0(J - 1) + \gamma_1 J(J - 1)^2 + \\
&\quad \left[\tfrac{2}{3} - \tfrac{2J}{2J+1}\right][\lambda_0 + \lambda_1(J - 1)] \\
b &= BJ(J + 1) - DJ^2(J + 1)^2 - [\gamma_0 + \gamma_1 J(J + 1)] + \\
&\quad \tfrac{2}{3}[\lambda_0 + \lambda_1 J(J + 1)] \\
c &= B(J + 1)(J + 2) - D(J + 1)^2(J + 2)^2 - \\
&\quad \left[\gamma_0(J + 2) + \gamma_1(J + 1)(J + 2)^2\right] + \\
&\quad \left[\tfrac{2}{3} - \tfrac{2(J+1)}{2J+1}\right][\lambda_0 + \lambda_1(J + 1)(J + 2)] \\
d &= 2\frac{\sqrt{J(J+1)}}{2J+1}\left[\lambda_0 + \lambda_1(J^2 + J + 1)\right]
\end{aligned} \quad (3)$$

The spectroscopic constants of O_2 used in the above equations are listed in Table 1.

Since O_2 is a homopolar molecule, it has no permanent electric dipole moment. Hence only magnetic dipole transitions are allowed; they obey the selection rules $\Delta N = 0, \pm 2$ and $\Delta J = 0, \pm 1$. The frequencies of the allowed transitions are obtained from the energy level determinations (Eqs. 2 and 3):

$$\begin{aligned}
(1, 1) \rightarrow (1, 0): &\quad \nu = (\gamma_0 + 2\gamma_1) + 2(\lambda_0 + 2\lambda_1) \\
(N, N) \rightarrow (N, N + 1): &\quad \nu = \nu_+(N) \\
(N, N) \rightarrow (N, N - 1): &\quad \nu = \nu_-(N) \\
(N + 2, N + 1) \rightarrow (N, N): &\quad \nu = \nu_R(N + 2) - \nu_-(N + 2) \\
(N + 2, N + 1) \rightarrow (N, N + 1): &\quad \nu = \nu_+(N) + \nu_R(N + 2) - \\
&\quad \nu_-(N + 2) \\
(N + 2, N + 2) \rightarrow (N, N + 1): &\quad \nu = \nu_+(N) + \nu_R(N + 2)
\end{aligned}$$

$$(4)$$

with

$$\begin{aligned}
\nu_R(N) &= \left(B - 2D\left(N^2 - N + 1\right) - \gamma_1 + \tfrac{2}{3}\lambda_1\right)(2N - 1) \\
\nu_\pm(N) &= \lambda_0 + \tfrac{1}{2}\gamma_0 - 4\gamma_1 + \left(\lambda_1 + \tfrac{5}{2}\gamma_1\right)\left(k^2 + k + 2\right) \pm \\
&\quad \left\{f(k) - (2k + 1)\left[B - 2D\left(k^2 + k + 1\right) - \gamma_1 + \tfrac{2}{3}\lambda_1\right]\right\} \\
f(k)^2 &= F^2 + k(k + 1)G^2 \\
F &= (2k + 1)\left[\left(B - \tfrac{1}{2}\gamma_0\right) - \left(2D + \tfrac{1}{2}\gamma_1\right)\right. \\
&\quad \left.\left(k^2 + k + 1\right) - \tfrac{3}{2}\gamma_1\right] - \frac{\lambda_0 + 1/3\lambda_1\left(7k^2 + 7k + 4\right)}{2k + 1} \\
G &= \frac{2\lambda_0 + 2\lambda_1\left(k^2 + k + 1\right)}{2k + 1} \\
k &= N \pm 1
\end{aligned}$$

$$(5)$$

Table 3. Upper level energies, frequencies and Einstein coefficients of the first 37 rotational lines of O$_2$

upper level (N, J)	lower level (N, J)	upper level energy (K)	ν (GHz)	A (s^{-1})
(1,1)	(1,2)	5.70	56.26476	5.82 10^{-10}
	(1,0)		118.7503	4.46 10^{-9}
(3,2)	(1,1)	23.39	368.4984	1.92 10^{-9}
	(1,2)		424.7632	2.40 10^{-8}
(3,3)	(1,2)	26.39	487.2494	8.45 10^{-9}
	(3,4)		58.44657	7.65 10^{-10}
	(3,2)		62.48626	9.10 10^{-10}
(5,4)	(3,3)	60.72	715.3933	6.44 10^{-9}
	(3,4)		773.8399	4.37 10^{-8}
(5,5)	(3,4)	63.62	834.1459	1.34 10^{-8}
	(5,6)		59.59091	8.30 10^{-10}
	(5,4)		60.30607	8.55 10^{-10}
(7,6)	(5,5)	114.56	1061.125	1.11 10^{-8}
	(5,6)		1120.715	6.34 10^{-8}
(7,7)	(5,6)	117.40	1179.880	1.82 10^{-8}
	(7,8)		60.43483	8.73 10^{-10}
	(7,6)		59.16428	8.17 10^{-10}
(9,8)	(7,7)	184.90	1406.373	1.60 10^{-8}
	(7,8)		1466.808	8.30 10^{-8}
(9,9)	(7,8)	187.70	1525.132	2.32 10^{-8}
	(9,10)		61.15053	9.08 10^{-10}
	(9,8)		58.32383	7.87 10^{-10}
(11,10)	(9,9)	271.76	1751.256	2.08 10^{-8}
	(9,10)		1812.407	1.02 10^{-7}
(11,11)	(9,10)	274.53	1870.019	2.80 10^{-8}
	(11,12)		61.80007	9.39 10^{-10}
	(11,10)		57.61253	7.60 10^{-10}
(13,12)	(11,11)	375.13	2095.780	2.56 10^{-8}
	(11,12)		2157.580	1.22 10^{-7}
(13,13)	(11,12)	377.86	2214.548	3.29 10^{-8}
	(13,14)		62.41119	9.68 10^{-10}
	(13,12)		56.96832	7.36 10^{-10}
(15,14)	(13,13)	494.98	2439.916	3.05 10^{-8}
	(13,14)		2502.328	1.42 10^{-7}
(15,15)	(13,14)	497.68	2558.691	3.78 10^{-8}
	(15,16)		62.99790	9.97 10^{-10}
	(15,14)		56.36344	7.14 10^{-10}

The Einstein coefficient of spontaneous emission for the transition u→l is:

$$A_{ul} = \frac{64\pi^4}{3hc^3}\nu^3\mu^2\frac{S_{ul}}{g_u} \qquad (6)$$

where ν is the frequency of the transition, $g_u = 2J_u+1$ is the statistical weight of the upper level, μ is the magnetic dipole moment (μ=2 Bohr magnetons) and the other symbols have their usual meaning. The line strengths S_{ul} for magnetic dipole transitions O$_2$ have been calculated by Tinkham & Strandberg (1955). The line strength values for $(N+2, N+1) \rightarrow (N, N)$ listed in Table VII of Tinkham & Strandberg are incorrect; correct values obtained from their equations (60) and (61) are listed in Table 2. The Einstein coefficients for absorption and stimulated emission B_{ul} and B_{lu} are computed with the usual expressions. The upper level energies, the frequencies and the probabilities of

spontaneous emission of the first 37 rotational transitions of O$_2$ are listed in Table 3. The energy level diagram of O$_2$, including the first six levels is presented in Fig. 1. The balloon-borne or satellite experiments and the lines they plan to observe are also indicated on the figure.

2.3.2. Collisional rates

We take into account the excitation and de-excitation of O$_2$ by collisions with H$_2$ and He, the most abundant species in parts of interstellar clouds where O$_2$ abundance is significant. We have used the theoretical calculations of the cross sections of excitation of O$_2$ by inelastic collisions with He obtained by Corey (1984), Orlikowsky (1986) and Corey et al. (1986). The collisional transitions between the levels (1, 0) and (N, N) are forbidden. For fixed ΔN, the collision rates are strongest for

Table 4. Column densities of oxygen-bearing species and population of the first six rotational levels of O_2 and emissivities of O_2 lines in three "standard" molecular clouds: A_V represents the visual extinction throughout the whole cloud.

	Diffuse cloud $A_V=1$ $n_H=500$ cm^{-3}		Translucent cloud $A_V=4$ $n_H=10^3$ cm^{-3}		Dark cloud $A_V=11$ $n_H=10^4$ cm^{-3}	
	$T=50$ K	thermal equilibrium	$T=25$ K	thermal equilibrium	$T=10$ K	thermal equilibrium
O (cm^{-2})	$1.7\ 10^{17}$	$1.7\ 10^{17}$	$5.3\ 10^{17}$	$5.3\ 10^{17}$	$7.0\ 10^{17}$	$7.0\ 10^{17}$
CO (cm^{-2})	$5.9\ 10^{13}$	$4.2\ 10^{13}$	$1.6\ 10^{17}$	$1.6\ 10^{17}$	$6.8\ 10^{17}$	$6.8\ 10^{17}$
O_2 (cm^{-2})	$2.6\ 10^{11}$	$1.8\ 10^{11}$	$1.2\ 10^{15}$	$8.5\ 10^{14}$	$1.7\ 10^{17}$	$1.7\ 10^{17}$
H_2O (cm^{-2})	$1.1\ 10^{12}$	$6.2\ 10^{12}$	$3.4\ 10^{14}$	$1.8\ 10^{14}$	$5.6\ 10^{15}$	$5.6\ 10^{15}$
OH (cm^{-2})	$1.0\ 10^{13}$	$6.6\ 10^{12}$	$9.5\ 10^{14}$	$6.8\ 10^{14}$	$1.2\ 10^{15}$	$1.2\ 10^{15}$
$N(O_2)/(2N(H_2)+N(H))$	$1.3\ 10^{-10}$	$8.8\ 10^{-11}$	$1.5\ 10^{-7}$	$1.0\ 10^{-7}$	$8.4\ 10^{-6}$	$8.4\ 10^{-6}$
$N(O_2(N=1, J=0))/N(O_2)$	$2.8\ 10^{-2}$	$4.0\ 10^{-2}$	$5.3\ 10^{-2}$	$7.6\ 10^{-2}$	0.12	0.12
$N(O_2(N=1, J=1))/N(O_2)$	$7.7\ 10^{-2}$	0.11	0.13	0.19	0.21	0.21
$N(O_2(N=1, J=2))/N(O_2)$	0.19	0.27	0.29	0.41	0.45	0.45
$N(O_2(N=3, J=2))/N(O_2)$	$4.4\ 10^{-2}$	$6.4\ 10^{-2}$	$6.4\ 10^{-2}$	$9.1\ 10^{-2}$	$5.4\ 10^{-2}$	$5.4\ 10^{-2}$
$N(O_2(N=3, J=3))/N(O_2)$	$9.0\ 10^{-2}$	0.13	0.11	0.15	$5.7\ 10^{-2}$	$5.7\ 10^{-2}$
$N(O_2(N=3, J=4))/N(O_2)$	0.23	0.33	0.22	0.31	$9.9\ 10^{-2}$	$9.9\ 10^{-2}$
O_2:(1, 1)→(1, 0) 119 GHz (K km s^{-1})	$3.2\ 10^{-6}$	$2.9\ 10^{-6}$	0.025	0.025	4.5	4.3
O_2:(3, 2)→(1, 1) 368 GHz (K km s^{-1})	$8.2\ 10^{-8}$	$6.1\ 10^{-8}$	$5.6\ 10^{-4}$	$1.8\ 10^{-4}$	0.065	0.053
O_2:(3, 2)→(1, 2) 425 GHz (K km s^{-1})	$7.7\ 10^{-7}$	$5.8\ 10^{-7}$	$5.2\ 10^{-3}$	$1.7\ 10^{-3}$	0.59	0.48
O_2:(3, 2)→(1, 2) 487 GHz (K km s^{-1})	$4.2\ 10^{-7}$	$3.1\ 10^{-7}$	$2.3\ 10^{-3}$	$6.6\ 10^{-4}$	0.17	0.14

$\Delta N = \Delta J$, i. e., for invariant spin ($\mathbf{J=N+S}$). We consider the collisional transitions $\Delta N=0$, 2, 4 and 6. Collisional rates are obtained from cross section determinations by using the following formula, which approximates cross section integration over a Maxwellian velocity distribution of collisional partners:

$$k_{lu} =< \sigma_{lu}v >\sim \left(3kT/\mu\right)^{1/2} \sigma_{lu} \qquad (7)$$

where T is the temperature, μ the reduced mass of the system O_2-He and k the Boltzmann constant.

De-excitation rates are obtained by the reversibility law:

$$k_{ul} = k_{lu} \frac{g_l}{g_u} \exp \left(\frac{E_l - E_u}{kT} \right) \qquad (8)$$

Following Black & Smith (1984), we adopt a temperature dependance for de-excitation rates as $T^{0.3}$. For use in numerical codes, it is practical to express collisional rates as simple functions of temperature. The collisional de-excitation rates O_2–He are listed in Appendix A.

Bergman (1995) has used a close-coupling calculation to compute the collisional cross-section O_2–He for a temperature range from 20 K to 100 K. His collisional rates (private communication) differ from our ones by a factor 0.02 to 2. A comparison between the O_2 line intensities obtained by Bergman and by our model is presented in Sect. 3.1 hereafter.

As it is usually done in the absence of any other information, H_2 is supposed to act, as a collision partner, in the same way as He at low temperature. Collisional rates O_2–H_2 have hence

been obtained by multiplying the corresponding O_2–He rates by the reduced mass factor: $\sqrt{\mu_{He}/\mu_{H_2}} \sim \sqrt{2}$.

For purpose of comparison, we have run models using the collisional rates adopted by Black & Smith (1984); the differences between the two sets of calculations are discussed hereafter.

2.3.3. Line emissivities

The simultaneous resolution of the statistical equilibrium equations for the rotational levels of O_2 and the chemical and thermal balance equations give the rotational population of O_2. Once this is obtained, it is possible to compute the intensity and the emissivity of rotational lines emerging from the cloud and to make direct comparison with observations or predictions. The main purpose of this paper is to compute, as a function of cloud parameters and their environments, the emissivities of O_2 lines that will be searched by the various balloon-borne and satellite experiments planed in the future.

The emissivity of the line connecting the rotational levels u and l and emerging normal to the cloud surface is obtained by integrating, over the whole line frequency, the intensity which is given by (e.g. Warin et al. 1996):

$$I_{ul}(x) = \frac{h\nu_{ul}}{4\pi} \frac{1}{\delta\nu_D} A_{ul}\phi(x) \int_0^{z_{max}} \left(\frac{S_{ul}(z')-I_{ul}^{ext}}{S_{ul}(z')} \right) n_l(z')\exp\left(-\tau_{ul}(z')\phi(x)\right) dz' \qquad (9)$$
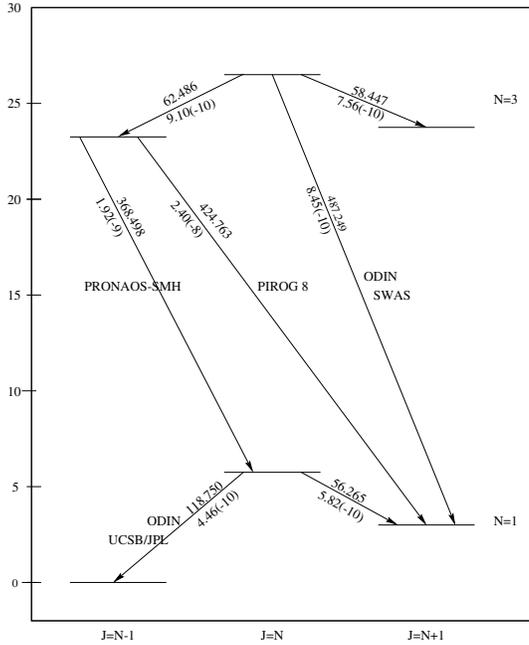
Fig. 1. The energy level diagram of the first six levels of O$_2$ and the transitions between these levels: The upper number on an arrow represents the frequency (GHz) of the transition, the lower one the Einstein coefficient of spontaneous emission (s^{-1}). The coming missions are also indicated.

where

$$S_{ul}(z) = \frac{2h\nu_{ul}^3}{c^2} \left(\frac{g_u n_l(z)}{g_l n_u(z)} - 1 \right)^{-1} \qquad (10)$$

is the source function at the current point z and

$$\tau_{ul}(z) = \frac{1}{\Delta \nu_D} \frac{c^2}{8\pi \nu_{ul}^2} A_{ul} \left(\frac{g_u}{g_l} N_l(z) - N_u(z) \right) \qquad (11)$$

is the line optical depth integrated over the whole line frequency. $n_i(z)$ is the local density of the molecule in the rotational level i and $N_i(z)$ is its column density from the current point z to the cloud surface. $\phi(x)$ is the normalized line profile; we adopted a Doppler profile including microturbulent broadening; all our model calculations have been performed by adopting for the most probable microturbulent velocity, a value $v_{turb} = 1$ km/s. $x = (\nu - \nu_0)/\Delta \nu_D$ is the frequency distance to the line center measured in Doppler widths. Throughout this paper, intensities will be expressed in terms of brightness temperature T^* and emissivities in K km s^{-1} by using the Rayleigh-Jeans approximation T^*=cI/2kν^2 and $\Delta\nu/\nu = \Delta v$/c.

3. Results of model calculations

Unless otherwise stated, in all model calculations presented hereafter the clouds are assumed to be homogeneous and submitted to the interstellar UV radiation field of Mathis et al. (1983); in some models this UV field has been multiplied by a scaling factor constant over the range 913–4000 Å. The cloud temperature distributions are either taken as uniform or obtained by solving the thermal balance equation. The cosmic-ray ionization rate of hydrogen is ζ_H=6.8 10^{-18} s^{-1}. For the chemical model, we adopted for the H$_3^+$ electronic recombination rate $\alpha_{H_3^+}$=9.75 10$^{-8}T^{-0.5}$ cm^{3}s^{-1} (Adams et al. 1984) much lower than the value typical for dissociative electronic recombination rates of molecular ions, but still larger than the negligibly low value ($\leq 10^{-11}$ cm^{3}s^{-1}) argued by Adams & Smith (1987). For the electronic recombination rate of H$_3$O$^+$, we adopted $\alpha_{H_3O^+}$=4 10$^{-5}T^{-0.5}$ cm^{3}s^{-1} with a branching ratio of 0.66 and 0.33 for OH and H$_2$O, respectively.

3.1. "Standard" diffuse, translucent and dark interstellar clouds

Following what has been done for the rotational excitation of CO (Warin et al. 1996), we first present the results of our model calculations for three "standard" interstellar clouds: a diffuse, a translucent and a dense dark cloud. For each cloud, we have run an isothermal model and a model in which the temperature distribution is obtained from the thermal balance. The cloud parameters, assumed to be representative of each type of cloud, are listed in Table 4 together with the column densities of the main oxygen-bearing species, the rotational population of O$_2$, expressed as the column density ratio $N(O_2(N,J))/N(O_2)$ of the first six rotational levels and the emissivities of the 119, 368, 425 and 487 GHz lines. For the elemental abundances, we adopted the solar values from the compilation of Anders & Grevesse (1989), i.e. H, He, C, O, S, Mg, Si and Fe respectively equal to 1, 9.8 10^{-2}, 3.6 10^{-4}, 8.5 10^{-4}, 1.6 10^{-5}, 3.8 10^{-5}, 3.5 10^{-5} and 4.7 10^{-5} with the same depletion of 10 for C and O for the three kinds of clouds, but an increasing depletion factor for sulfur and metals of 10, 100 and 10^4 for diffuse, translucent and dark clouds, respectively. The adopted depletions of carbon and oxygen are consistent with what can be expected in dense opaque clouds. The main reason to adopt the same depletion in more diffuse clouds, where elements are probably less depleted is to perform our model calculations with an identical C/O ratio (see discussion later) for all kind of clouds. The adopted depletion of sulfur is more questionable in view of recent observations by HST (Savage & Sembach 1996). Preliminary calculations including the chemistry of sulfur (and nitrogen) seems to indicate that it has little influence on the abundance of O$_2$.

As expected with the "normal" value C/O∼0.4, the most abundant oxygen-bearing species are O and CO. It is interesting to point out that atomic oxygen remains the most abundant oxygen bearer, even in dark clouds. After O and CO, molecular oxygen becomes the most abundant oxygen-bearing species in the translucent cloud and has an abundance comparable with that of CO in the dark cloud. It must be noted that, with the sensitivity expected for the receivers of the forthcoming missions (see below), O$_2$ will be observable only in dense molecular cloud; its observation in diffuse or translucent clouds would need more sensitivity. According to the line emissivities computed for dark clouds (Table 4), and using the usual relation:

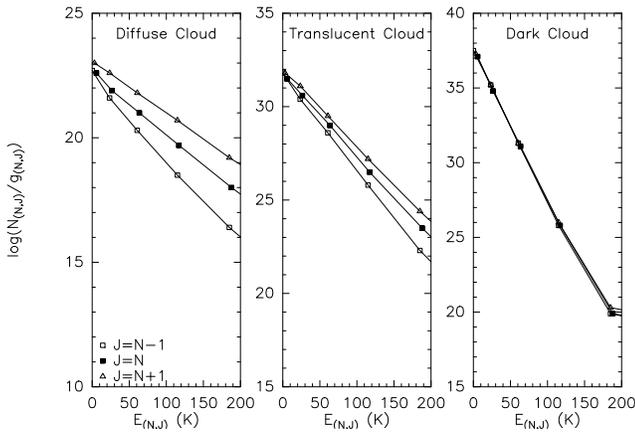$$\sigma = 2T_{sys}/(B\tau)^{1/2} \qquad (12)$$

Fig. 2. Log($N_{(N,J)}/g_{(N,J)}$) as a function of the rotational level energy of O$_2$ for the three isothermal standard clouds presented in Table 4

where σ is the root mean square deviation, T$_{sys}$ is the system temperature, B the noise equivalent bandwidth per channel and τ the integration time, a 5σ detection of O$_2$ needs about 35 hours of integration at 487 GHz with ODIN (T$_{sys}$=3000 K, B=1 MHz) and 10 h with SWAS (T$_{sys}$=2080 K, B=1.6 MHz), about 12 min at 425 GHz with PIROG (T$_{sys}$=500 K, B=400 kHz), about 2 h at 368 GHz with PRONAOS (T$_{sys}$=300 K, B=1 MHz) and less than 1 min at 119 GHz with the HEMT receiver of ODIN (T$_{sys}$=300 K, B=150 kHz), assuming no beam dilution (eg: beamsize of ODIN $\sim$ 9' at 119 GHz).

A way to represent the rotational population of O$_2$ is shown in Fig. 2 where the variations of the quantity Log($N_{(N,J)}/g_{(N,J)}$) are plotted as a function of the rotational level energy. For the diffuse and translucent clouds, the levels $J = N$+1, N, N-1 seem to behave as three separate populations not very far from LTE but with slightly different rotational temperatures T_{rot}= 48, 42 and 34 K for the series $J=N$+1, $J=N$ and $J=N$-1, respectively, for the diffuse cloud with T_{kin}=50 K, and T_{rot}=26, 25 and 21 K for the same series in the translucent cloud with T_{kin}=25 K. In the dark cloud model, thermalization is achieved for all rotational levels up to N=9 with $T_{rot}=T_{kin}$=10 K.

For comparative purposes, we have calculated the rotational population of O$_2$ with the collisional rates used by Black & Smith (1984, hereafter "BS rates"). The comparison is shown in Table 5 for the first fifteen levels of O$_2$. For the diffuse cloud, differences already appear from the first levels (N=1, 3) which are more populated with the BS rates at the detriment of the upper levels ($N \geq 5$). For the translucent cloud, the two series of collisional rates give similar results for the levels N=1, 3. For the dense cloud, except for the ground level (N=1, J=0), there is a good agreement between the two sets of results which differ by less than 30 % up to N=5: these levels are near the thermalisation. The ground level is underpopulated by nearly a factor two when BS rates are used: this comes from the fact that collisional transfer between the (N=1, J=0) and (N=1, J=1) levels is allowed by Black & Smith (1984) and is efficient in destroying the ground level; conversely, this transition is forbidden in our model and thermalisation is completely achieved for the three

N=1 levels (see Fig. 2). A glance at Table 5 also shows that using the BS rates leads to an underestimation of the population of excited levels above (N=5, J=4): this is because collisional transitions for $\Delta N > 2$ are not taken into account by Black & Smith while they are present (see Sect. 2.3.2), allowing to populate excited levels through collisional excitation of lower lying levels.

To further compare our model calculations with previous works, Table 6 displays the rotational line emissivities obtained by Bergman (1995) and by us. For a translucent cloud, the two models give similar results and Bergman's line emissivities are at most a factor 2 lower than ours, while, for a dark cloud in which the thermalisation is completely achieved for the levels $N = 1$ and $N = 3$, the line emissivities are equal to within 15 % in the two models.

3.2. O$_2$ abundance and line emissivities as a function of visual extinction thoughout the whole cloud

3.2.1. The effect of the density

The first series of models represents homogeneous clouds of total hydrogen densities n_H= 500, 10^3, 10^4 and 10^5 cm^{-3} and the temperature distributions are obtained from the thermal balance equation. All the clouds are submitted to the UV radiation field of Mathis et al. (1983) and all models were run with the elemental abundances of the translucent cloud (see above) which correspond to a "standard" C/O ratio of 0.4 and metals and sulphur depleted by a factor 100 with respect to solar values. Fig. 3 displays the abundances, in terms of the column density ratio N(X)/(N(H)+N(H$_2$)), of the main oxygen-bearing species O, OH, H$_2$O, O$_2$ and CO throughout clouds of various visual extinction. It is interesting to note that the conversion of oxygen into molecular form is not complete since atomic oxygen remains the dominant species up to A_V=8–9 whatever the density and still represents between 20 and 30 % of the available gas phase oxygen in the most opaque clouds computed here (A_V= 10 to 30); the atomic oxygen abundance is comparable to that of CO and still larger than that of O$_2$. Except for OH, the molecular abundances are more sensitive to the density in diffuse and translucent clouds than in more opaque clouds: as expected, the general tendency is an increase of molecular abundances and a corresponding decrease of atomic form with increasing density. An important exception is OH whose abundances scales nearly as n_H^{-1} beyond A_V=8; this is essentially due to its very efficient conversion into molecular oxygen through reaction (1) which is both the main destruction process of OH and the main formation process of O$_2$. The effect of varying the rate coefficient of this reaction on both OH and O$_2$ abundances is discussed later. Finally our model calculations confirm previous results indicating the large amount of molecular oxygen produced in opaque clouds: beyond A_V=10, O$_2$ takes between 20 and 35 % of the gas phase oxygen. The abundance ratio O$_2$/CO, not very sensitive to density, ranges from 0.2 to 0.4 as A_V increases from 10 to 30 and stays constant around 0.4 for larger opacities.
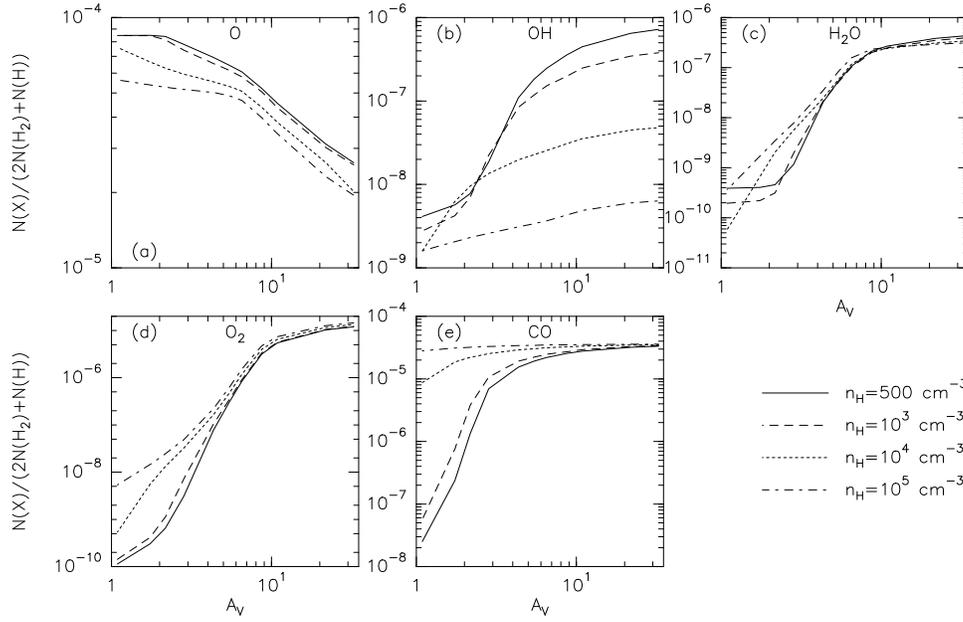
Fig. 3a–e. Abundances, in terms of $N(X)/(N(H)+N(H_2))$, of oxygen-bearing species as a function of the total visual extinction throughout different kinds of clouds and as a function of hydrogen density. Temperatures are computed from thermal balance: **a** O, **b** OH, **c** H_2O, **d** O_2, **e** CO

Table 5. Population of the first fifteen rotational levels of O_2 in three isothermal "standard" molecular clouds for the two series of collisional rates: the one adopted here and those adopted by Black & Smith (1984) (BS84)

	Diffuse cloud $A_V=1$ $n_H=500$ cm^{-3} $T=50$ K		Translucent cloud $A_V=4$ $n_H=10^3$ cm^{-3} $T=25$ K		Dark cloud $A_V=11$ $n_H=10^4$ cm^{-3} $T=10$ K	
	this model	BS84	this model	BS84	this model	BS84
$N(O_2(N=1, J=0))/N(O_2)$	0.028	0.061	0.053	0.065	0.12	0.076
$N(O_2(N=1, J=1))/N(O_2)$	0.077	0.17	0.13	0.17	0.21	0.17
$N(O_2(N=1, J=2))/N(O_2)$	0.19	0.32	0.29	0.36	0.45	0.51
$N(O_2(N=3, J=2))/N(O_2)$	0.044	0.099	0.064	0.093	0.054	0.059
$N(O_2(N=3, J=3))/N(O_2)$	0.090	0.13	0.11	0.12	0.057	0.063
$N(O_2(N=3, J=4))/N(O_2)$	0.23	0.18	0.22	0.17	0.096	0.11
$N(O_2(N=5, J=4))/N(O_2)$	0.023	0.012	0.018	7.8e-3	$2.1\ 10^{-3}$	$1.8\ 10^{-3}$
$N(O_2(N=5, J=5))/N(O_2)$	0.057	0.014	0.033	8.5e-3	$2.1\ 10^{-3}$	$1.6\ 10^{-3}$
$N(O_2(N=5, J=6))/N(O_2)$	0.15	0.018	0.067	0.011	$3.4\ 10^{-3}$	$2.6\ 10^{-3}$
$N(O_2(N=7, J=6))/N(O_2)$	$5.3\ 10^{-3}$	$9.2\ 10^{-4}$	$1.7\ 10^{-3}$	$1.2\ 10^{-4}$	$1.2\ 10^{-5}$	$5.2\ 10^{-6}$
$N(O_2(N=7, J=7))/N(O_2)$	0.021	$1.1\ 10^{-3}$	$4.2\ 10^{-3}$	$1.2\ 10^{-4}$	$1.3\ 10^{-5}$	$4.5\ 10^{-6}$
$N(O_2(N=7, J=8))/N(O_2)$	0.063	$1.6\ 10^{-3}$	$9.6\ 10^{-3}$	$1.6\ 10^{-4}$	$2.0\ 10^{-5}$	$6.8\ 10^{-6}$
$N(O_2(N=9, J=8))/N(O_2)$	$8.4\ 10^{-4}$	$3.9\ 10^{-4}$	$7.2\ 10^{-5}$	$1.1\ 10^{-5}$	$4.3\ 10^{-8}$	$4.2\ 10^{-7}$
$N(O_2(N=9, J=9))/N(O_2)$	$4.9\ 10^{-3}$	$5.3\ 10^{-4}$	$2.5\ 10^{-4}$	$1.3\ 10^{-5}$	$5.0\ 10^{-8}$	$3.6\ 10^{-7}$
$N(O_2(N=9, J=10))/N(O_2)$	0.018	$7.7\ 10^{-4}$	$6.8\ 10^{-4}$	$1.9\ 10^{-5}$	$8.2\ 10^{-8}$	$5.5\ 10^{-7}$

Table 6. O_2 line emissivities (K km s^{-1}) in a translucent cloud and a dark one obtained by Bergman (B95) and by our model

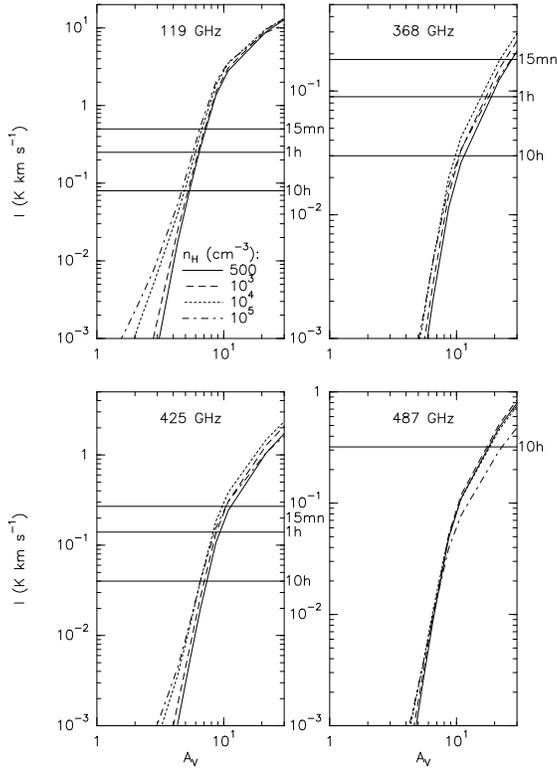|	Translucent cloud $n_H=10^3$ cm^{-3} $T=50$ K $N(O_2)=10^{15}$ cm^{-2} $\Delta V=1$ km/s		Dark cloud $n_H=2\ 10^4$ cm^{-3} $T=50$ K $N(O_2)=10^{17}$ cm^{-2} $\Delta V=1$ km/s	
	B95	this model	B95	this model
$(1, 1) \rightarrow (1, 0)$	0.0099	0.0114	2.08	2.29
$(1, 1) \rightarrow (1, 2)$	0.0035	0.0055	1.14	1.30
$(3, 2) \rightarrow (1, 2)$	0.0028	0.0039	0.62	0.66
$(3, 2) \rightarrow (1, 1)$	0.0003	0.0004	0.07	0.07
$(3, 3) \rightarrow (1, 2)$	0.0016	0.0018	0.22	0.22
$(3, 3) \rightarrow (3, 2)$	0.012	0.012	1.32	1.30
$(3, 3) \rightarrow (3, 4)$	0.0036	0.0076	1.14	1.23

Fig. 4. Emissivities of O_2 lines as a function of the total visual extinction throughout different kinds of clouds and as a function of density. Horizontal lines give, for various integration times, the lowest emissivity that can be reached with a signal-to-noise ratio of 5 by the receivers of the ODIN (119 GHz and 487 GHz), PRONAOS (368 GHz) and PIROG (425 GHz) experiments

The predicted emissivities of O_2 lines at 119, 368, 425 and 487 GHz, defined as $I = \int I(\nu)d\nu$, where $I(\nu)$ is given by Eq. (10) above, are plotted in Fig. 4. The horizontal lines on the figure give, for various integration times, the lowest emissivity that can be reached with a signal-to-noise ratio of 5 by the receiver of the ODIN (119 and 487 GHz), PRONAOS (368 GHz) and PIROG8 (425 GHz) experiments. They are obtained from relation (12). Parameters T_{sys} and B adopted for the receivers have been given in Sect. 3.1.

The emissivities are nearly insensitive to density, except for the 119 GHz lines in low opacity clouds but with values too low to be accessible to observations. They however strongly depend on the cloud visual extinction, exhibiting orders of magnitude variations as A_V change by only a few units. Detection of O_2 by PRONAOS and PIROG appears possible only in dense dark clouds after an hour of integration, while 10 hours are required for SWAS and more than 10 hours for the 487 GHz receiver of ODIN. The 119 GHz receiver, much more sensitive, appears to be able to detect O_2 in translucent clouds (A_V=5) with the same integration time, provided there is no beam dilution.

3.2.2. The effect of temperature

To study the effect of temperature, we have run a series of homogeneous cloud models (n_H=10^4 cm^{-3}) with various uniform temperatures T= 10, 25, 50, 75 and 100 K. All models were run with elemental abundances of the dark cloud (i.e. C/O = 0.4 and metals and sulphur depleted by a factor 10^4 with respect to solar values). The abundances of the main oxygen-bearing species are plotted on Fig. 5. The abundances are not very sensitive to the temperature except for H_2O and OH, the abundances of which increase with increasing temperature in diffuse and translucent clouds in the case of H_2O and in all kinds of clouds in the case of OH. Increasing the temperature increases the efficiency of production of O^+ (throught the slightly endothermic charge transfer reaction $H^+ + O \rightarrow O^+ + H$) whose reaction with H_2 initiates the formation of oxygen hydrides.

The predicted emissivities of O_2 lines at 119, 368, 425 and 487 GHz are plotted in Fig. 6 with the lowest accessible emissivity (horizontal lines) as defined in Fig. 4. Unlike the overall O_2 abundance, its rotational population (partly controlled by collisions), and consequently the line emissivities, are quite sensitive to the temperature. The population of the level $(N, J) = (1, 1)$, from which the 119 GHz line originates, is maximum near 7 K; the population of the (3, 2) and (3, 3) levels, from which the three other lines originate, reach their maximum at slightly higher temperature of 25 K and 28 K respectively. Whatever the kind of cloud, the 119 GHz line has the strongest emissivity; it however decreases as the temperature increases. The three other lines show a maximum emissivity around 25 K; the 368 and 487 GHz lines appear to be detectable by the receivers of PRONAOS and SWAS, respectively, after one hour of integration in clouds with $A_V \sim 10$. In the same conditions, the PIROG 8 receiver is able to detect the 425 GHz in less opaque clouds with $A_V \sim 6$–7.

3.2.3. The influence of the UV radiation field

A series of homogeneous ($n_H = 10^4$ cm^{-3}) cloud models has been computed in which the incident ultraviolet radiation field is multiplicated by a factor $f_{UV} = 10$, 100 and 10^3 to simulate molecular clouds near regions of star formation. All models were run with the dark cloud elemental abundances and the temperature distributions are obtained from the thermal balance equation. Fig. 7 displays the abundances of the main oxygen-bearing species versus the visual extinction. As expected, the increase of the UV field causes a drastic depletion of molecules, by several orders of magnitude, until fairly large ($A_V \sim 10$–20) cloud opacities are reached. For OH, H_2O and O_2, photodestruction remains important up to large visual extinction ($A_V = 20$). The CO molecule is much more resistant to photodissociation and its abundance is not sensitive to the intensity of the external UV radiation field (at least up to $f_{UV} = 1000$) for cloud opacities larger than 6. As discussed in Warin et al. (1996), self-shielding is very efficient for CO which is destroyed through absorption of photons within discrete lines towards predissociated levels of electronic Rydberg states.
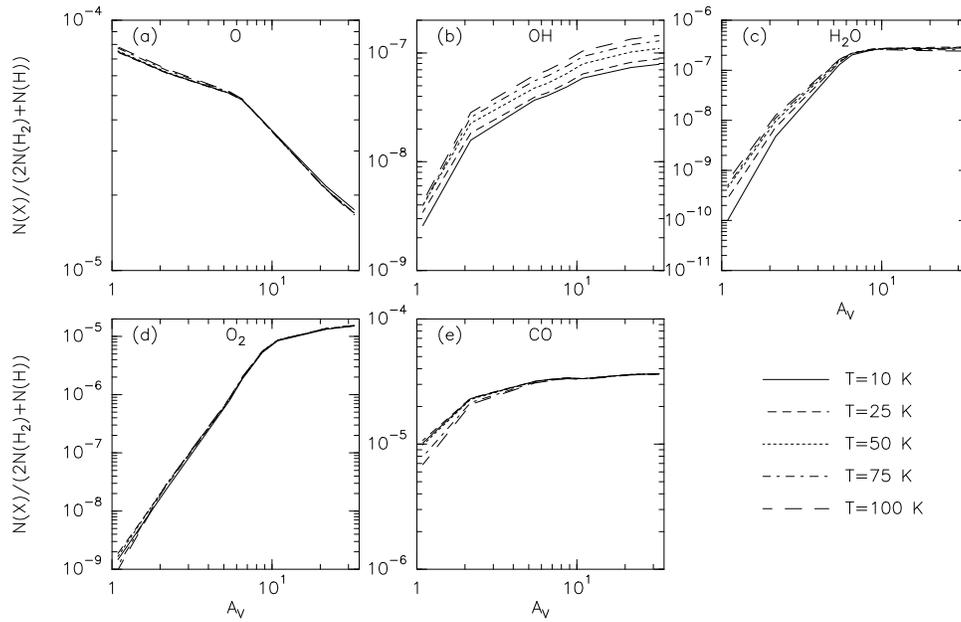
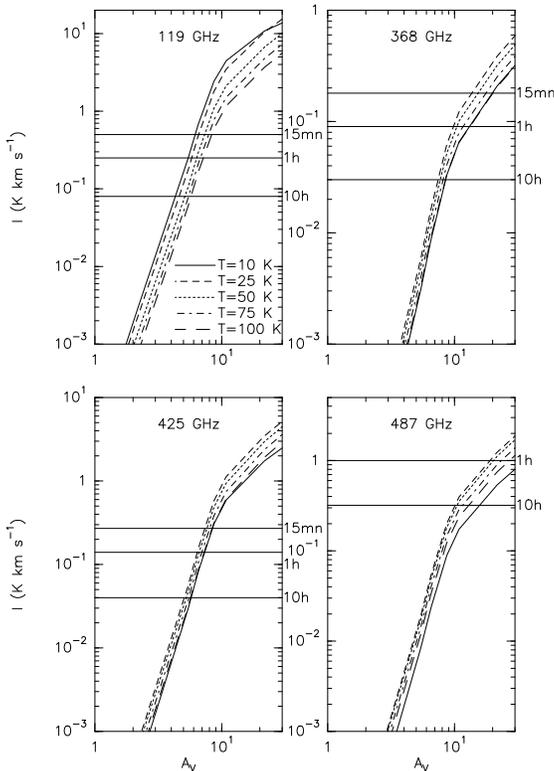**Fig. 5a–e.** Abundances, in terms of $N(X)/(N(H)+N(H_2))$, of oxygen-bearing species as a function of the total visual extinction throughout different kinds of clouds and as a function of temperature in homogeneous clouds with $n_H=10^4$ cm^{-3}: **a** O, **b** OH, **c** H_2O, **d** O_2, **e** CO

Fig. 6. Emissivities of O_2 lines as a function of the total visual extinction throughout different kinds of clouds and as a function of temperature. Horizontal lines have the same meaning than in Fig. 4

Due to the reduced abundance, the predicted emissivities of O_2 lines, plotted in Fig. 8, are seriously decreased so as to become undetectable in most clouds. If the UV field is enhanced by a factor of 1000, 10 hours of integration appears necessary with the ODIN receiver to detect the 119 GHz line in clouds with $A_V = 10$. With the same integration time, the three other lines are observable only in larger opacity clouds ($A_V = 20$). Such a large integration time is possible with satellites such as ODIN and SWAS but appears excluded for balloon-borne experiments such as PRONAOS and PIROG 8.

3.2.4. The influence of the C/O elemental abundance ratio

Up to now, our model calculations have been performed with "standard" elemental abundances, i.e. with a carbon abundance much lower (by more than a factor two) than that of oxygen. This, together with the assumption of steady-state chemistry, explains the rapid increase of the O_2 abundance, and, to a lesser extent that of OH and H_2O, with cloud opacity. Indeed, in the steady-state, the conversion of gas-phase carbon into CO is very efficient so that nearly all carbon is in form of CO beyond $A_V = 5$–10 (depending on the density and the UV field as shown in Fig. 3e and 7e). If oxygen is more abundant than carbon, there remains enough gas phase oxygen to build other molecules, although the transformation of oxygen into molecular form is not complete since atomic oxygen remains abundant (see above results). If, conversely, oxygen is less abundant than carbon, the CO abundance is limited by the available gas phase oxygen, so that there is no more oxygen to build other molecules.

To our knowledge, there is no systematic study of the influence of the C/O abundance ratio on the chemical composition of interstellar clouds except for a paper by Langer & Graedel (1989) who computed the chemical composition of dense molecular clouds for three values of the C/O ratio of 0.7,
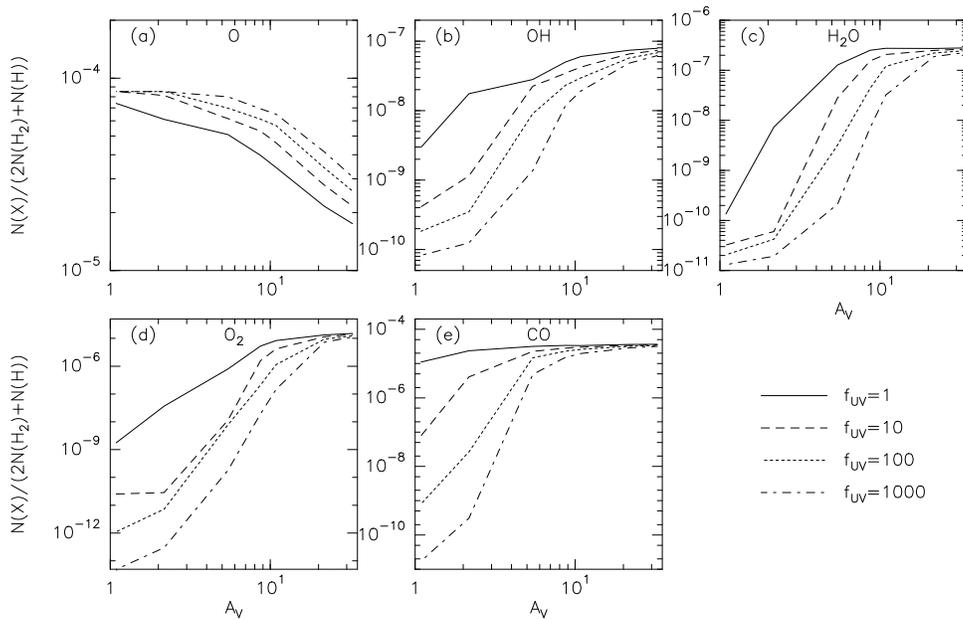
Fig. 7a–e. Abundances, in terms of $N(X)/(N(H)+2N(H_2))$, of oxygen-bearing species as a function of the total visual extinction throughout different kinds of clouds and as a function of UV radiation field in homogenous clouds with $n_H=10^4\,cm^{-3}$. Temperatures are computed from thermal balance: **a** O, **b** OH, **c** H_2O, **d** O_2, **e** CO

1.1 and 1.3. To compensate for this lack, we have run a series of cloud models with various C/O ratios in the range 0.1 to 2, the oxygen abundance being fixed as $8.5\ 10^{-5}$. All models have the same constant density ($n_H = 10^4\ cm^{-3}$) and temperature ($T = 10$ K) and metals and sulfur depleted by a factor 10^4. Fig. 9 and 10 display, as a function of visual extinction and of the C/O abundance ratio, the abundances of the main oxygen-bearing species and the emissivities of the O_2 lines, respectively. The strong dependence of the abundances on the C/O ratio is clearly shown in Fig. 9 and this is true whatever the type of the cloud, diffuse, translucent or dense. As the C/O increases, i.e. as the carbon abundance increases since the oxygen one is fixed, the CO abundance increases in the same proportion until C/O = 1; beyond this value, CO continues to increase only in low opacity clouds, while, in more opaque clouds, its abundance stays constant nearly equal to that of the available gas-phase oxygen. At the same time, the abundance of OH, H_2O and O_2 decrease with increasing C/O. The drop of their abundances is more or less steep, depending on the cloud opacity and, above all, on the fact that carbon is less or more abundant than oxygen. For a typical dark cloud ($A_V = 10$), as C/O increases from the standard value of 0.4 to 1, i.e. a factor of two, the OH, H_2O and O_2 abundances drop by a factor 3, 100 and 150, respectively; another factor of 2 increase of C/O, from 1 to 2, causes an even larger drop of the abundances of these three species by further factors 10, 25 and 240, respectively.

The effect of increasing the C/O ratio on O_2 line emissivities is shown on Fig. 10: with the sensitivity of the receivers of the forthcoming experiments, none of the O_2 lines is detectable with a C/O ratio around 1 or larger; the exception is the ODIN satellite which could detect the 119 GHz in opaque clouds ($A_V \sim 20$–30) up to C/O ~ 1 after 10 hours of integration; provided that C/O ≤ 0.7, such clouds are accessible to the PRONAOS or PIROG experiments with 1 hour of integration
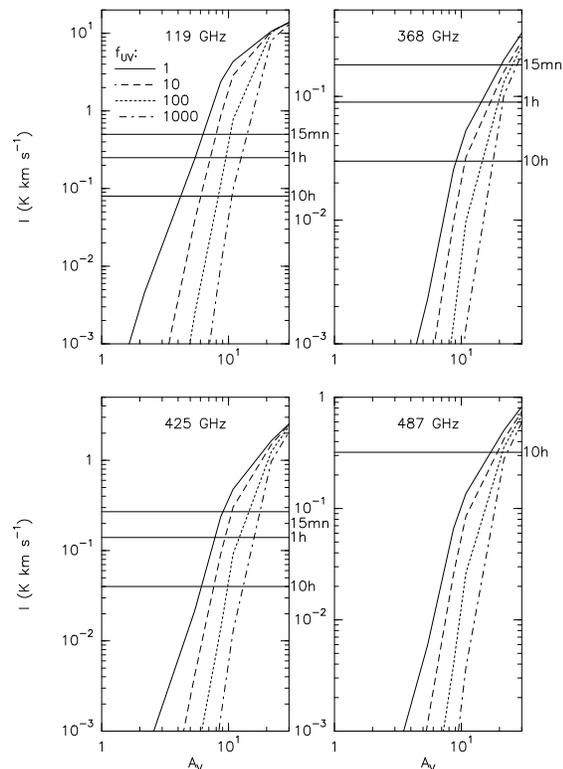

Fig. 8. Emissivities of O_2 lines as a function of the total visual extinction throughout different kinds of clouds and as a function of UV radiation field. Horizontal lines have the same meaning than in Fig. 4
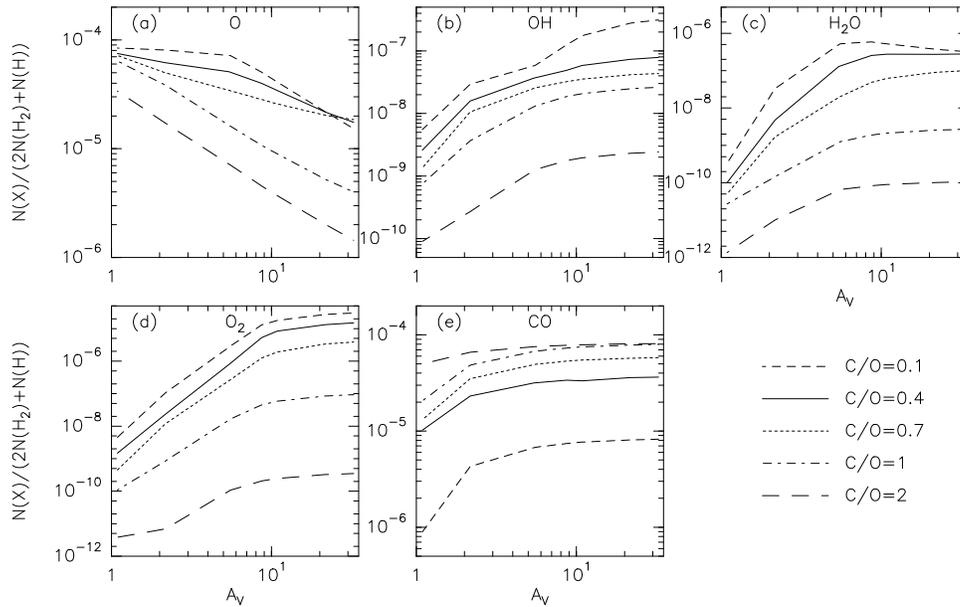
Fig. 9a–e. Abundances, in terms of $N(X)/(N(X)+N(H_2))$, of oxygen-bearing species as a function of the total visual extinction throughout different kinds of clouds and as a function of C/O ratio for homogeneous isothermal clouds (n_H=10^4 cm^{-3}, T_{kin}=10 K). The abundance of oxygen is constant: X_O=8.5 10^{-5}. **a** O, **b** OH, **c** H$_2$O, **d** O$_2$, **e** CO

and to SWAS with 10 hours of integration. Because of the very strong sensitivity of the O$_2$ abundance which decreases by more than four orders of magnitude as C/O increases from 0.4 to 2, detection of O$_2$ lines could well help to determine the C/O ratio and its possible variations throughout the interstellar medium. Tentative detection of the 368 and 425 GHz lines in absorption from the ground (at IRAM) have been performed by Combes & Wiklind (1995) in an extragalactic molecular cloud where, because of the redshift, lines are not absorbed by atmospheric lines. These observations gave negative results with an upper limit $N(O_2)/N(CO) \leq 0.046$ (at 3σ detection), somewhat lower than previous determinations in extragalactic clouds. Interpreting this as an overabundance of carbon with respect to oxygen would give C/O $\geq$ 0.7–0.8 according to Fig. 9. Apart from the increase of the UV radiation field or a large C/O ratio, alternative models exist which can explain a very low O$_2$ abundance. Chièze & Pineau des Forêts (1989) suggested a possible mixing between the outer layers and the inner part of molecular clouds due to turbulence. This would increase the abundances of ions such as C$^+$ in the core of the cloud causing a efficient destruction of O$_2$. More recently, model calculations by Le Bourlot et al. (1995) indicated the possible existence of two stable phases for the chemical composition of molecular clouds, a low ionization phase similar to that obtained in our model and a high ionization phase with larger abundances of ions such as C$^+$ and H$^+$ and an O$_2$ fractional abundance 100 times lower. Another possibility to reduce the abundance of O$_2$, as well as that of many other molecules, is to allow them to freeze on the surfaces of cold grains: the possibility to observe solid O$_2$ and other oxygenated species such as H$_2$O, CO and CO$_2$, with ISO has been suggested by Ehrenfreund et al. (1992). Up to now, presence of O$_2$ adsorbed on grain surfaces has not been observed. Finally, the clumpy structure of molecular clouds helps the penetration of UV photons (Boissé 1990) so that the O$_2$ abundance can be re-

duced by a factor 3 with respect to uniform clouds as suggested by recent models (Spaans 1996 and private communication).

3.3. The influence of the reaction $O + OH \rightarrow O_2 + H$

For this reaction, which is the main way to form O$_2$, we have adopted a theoretical determination of its rate coefficient (see Sect. 2.2) which seems to indicate the presence of a small activation barrier: $k_1 \alpha \exp(-E_A/T)$ with E_A = 6 K. Up to now, no measurements have been performed down to interstellar temperatures so that the presence of a larger activation barrier cannot be excluded. To check this, we have run dense cloud models ($n_H = 10^4$ cm^{-3}) by assuming an activation barrier of 60 K for the reaction (1); we also adopted a low temperature (T = 10 K) for which the presence of an activation barrier, even low, has more importance for the chemistry. The abundances of OH, H$_2$O and O$_2$, computed with E_A = 6 and 60 K in clouds of various extinctions are plotted in Fig. 11 (O and CO, not sensitive to E_A, are not plotted). We confirm the result pointed out by Black & Smith (1984) that the O$_2$ abundance is fairly insensitive to the exact value of k_1 in opaque clouds, beyond A_V = 6. This is because, in dense opaque clouds, reaction (1) is also the main destruction process of OH with the consequence that its local density scales as $1/k_1$ so that the production rate of O$_2$, proportional to $k_1 n_{OH}$, becomes independant of k_1. At 10 K, the decrease of k_1 by a factor 200 as E_A increases from 6 to 60 K is nearly exactly compensated by the corresponding increase of the OH abundance by the same factor (Fig. 11a) and the O$_2$ abundance is pratically unchanged (Fig. 11c). As shown in Fig. 11a, as the opacity of the cloud decreases, going to translucent and diffuse clouds, the OH abundance becomes less and less sensitive to the rate coefficient of the reaction (1) which is progressively replaced by reactions with H$^+$, C$^+$ and C to destroy OH; reaction (1) remains however the main route to O$_2$ whose abundance decreases with k_1, but becomes too low to be
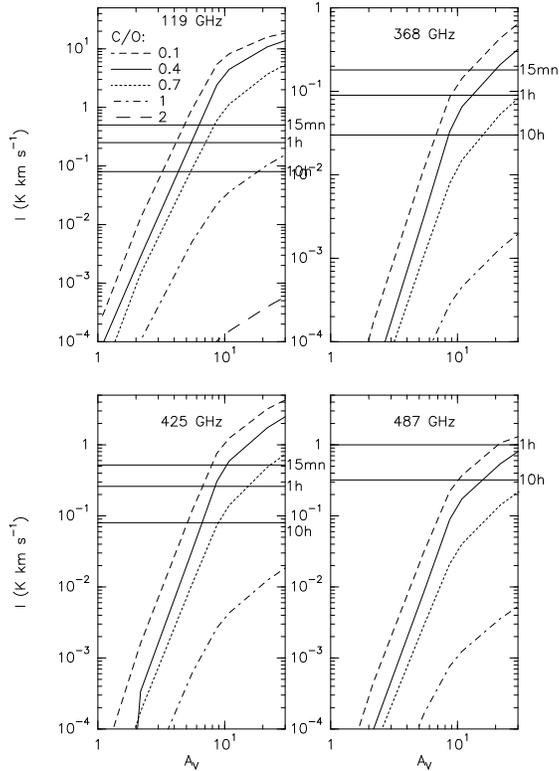
Fig. 10. Emissivities of O_2 lines as a function of the total visual extinction throughout different kinds of clouds and as a function of C/O ratio for constant oxygen abundance (X_O=8.5 10^{-5}). Horizontal lines have the same meaning than in Fig. 4

Fig. 11a–c. Abundance of OH (**a**), H_2O (**b**) and O_2 (**c**) for dense cold clouds (n_H=10^4 cm^{-3} and T=10 K) as a function of the total visual extinction throughout different kinds of clouds and as a function of the activation barrier E of the rate coefficient of the reaction OH+O→O_2+H

Fig. 12. Cooling rates of O_2 and CO for opaque clouds ($A_V \sim 30$) as a function of the optical depth and the hydrogen density. The cooling rate of a species is divided by n_H.

detected through observations in the millimeter or submillimeter range. Our previous conclusions about the detectability of O_2 are not altered by the exact value of the rate coefficient of reaction (1). The sensitivity of the OH and O_2 abundances on a possible activation barrier on reaction (1) depends of course on the cloud temperature. At higher temperatures, e.g. T=50 K, larger activation barriers E_A = 200 and 300 K should be necessary to reduce the OH abundance in opaque clouds by a factor 30 and 100 respectively, the O_2 abundance remaining essentially unaffected.

3.4. Cooling efficiency of O_2 lines and their influence on the thermal balance of molecular gas

Our model calculations show that under favourable conditions (C/O < 1 and a not too high UV field), O_2 appears to be one of the most abundant interstellar molecules, with an abundance comparable to that of CO in dense opaque clouds. Furthermore, the excitation energies of its first rotational levels are low enough to be collisionally excited even at low interstellar cloud temperatures. At last, our calculations indicate that the O_2 lines are optically thin. Therefore, O_2 must be an efficient cooling agent of molecular gas, at least in dense and cold clouds. This is clearly shown on Fig. 12 where the cooling rates by O_2 and CO are plotted as a function of optical depth within clouds of
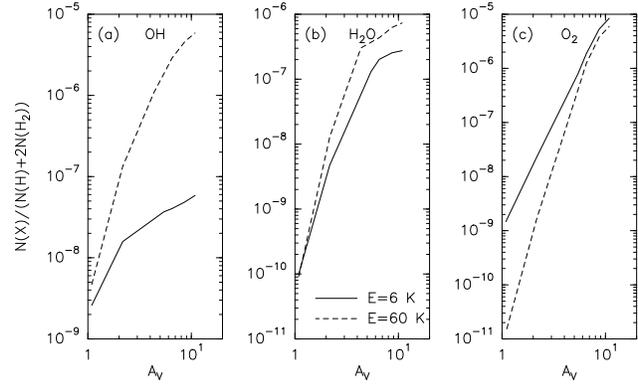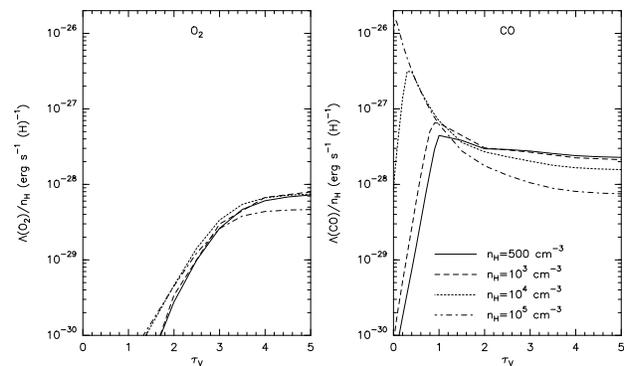
various densities. Cooling by C, C$^+$ and O are not represented because they are negligibly low as soon as $\tau_V \geq 0.5$. As soon as the optical depth is larger than 4, the O_2 cooling becomes comparable to that of CO, to within a factor 2. Typically, in a core of a dense dark cloud, the (1, 1)–(1, 0), (3, 2)–(1, 2) and (3, 3)–(1, 2) lines at 119, 425 and 487 GHz contribute to 10, 52 and 22 %, respectively, of the cooling by O_2.

Of course, as for its abundance, the O_2 cooling efficiency will strongly depend on the C/O abundance ratio. This is illustrated in Fig. 13 where are plotted, as a function of optical depth within a dense dark cloud ($n_H = 10^4$ cm^{-3}), the CO and O_2 abundances, their cooling rates and the resulting temperature, for two extreme values C/O = 0.1 and 1. With the low C/O ratio, O_2 becomes the dominant species and cooling agent in the core of the cloud, lowering the temperature down to 7 K, nearly 3 K below the temperature obtained when CO dominates the cooling. As expected and due to its low abundance, O_2 however does not play any role when C/O = 1.

Despite its potential importance, O_2 cooling has often been neglected in models of interstellar clouds, except for the work done by Goldsmith & Langer (1978, hereafter GL78) who made
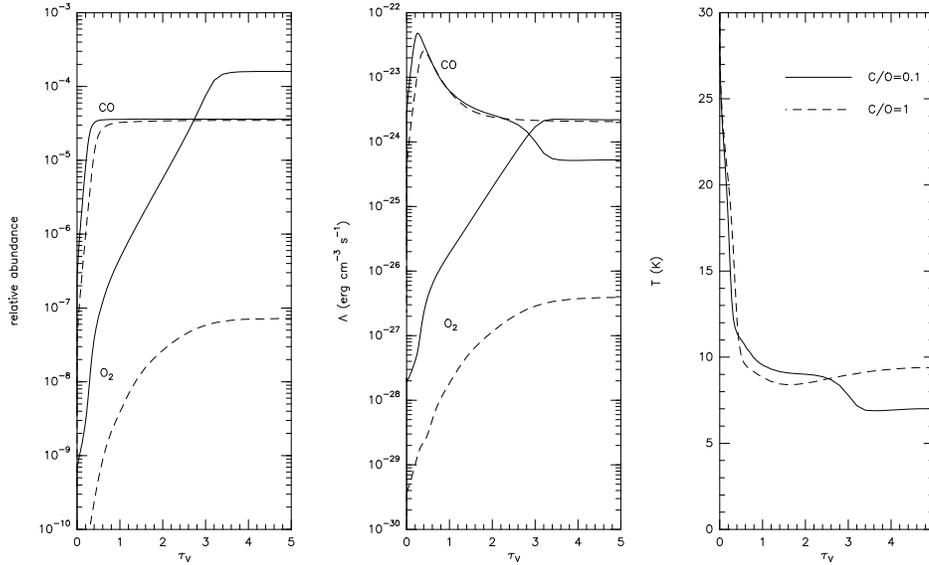
Fig. 13. The abundance and cooling rate of O_2 and CO and the temperature profile throughout dark clouds ($A_V = 11$) at $n_H = 10^4$ cm^{-3} and $X_C = 3.6 \ 10^{-5}$ for C/O ratio of 0.1 and 1 as a function of the optical depth

Table 7. Comparison of the cooling efficiencies of O_2 and CO obtained in Goldsmith & Langer (1978, refered to as GL78) and in our model ($A_V \sim 30$)

		$\Lambda(O_2)/n(O_2)$ (erg s^{-1} $(O_2)^{-1}$)	$\Lambda(CO)/n(CO)$ (erg s^{-1} $(CO)^{-1}$)
$n_H = 10^3$ cm^{-3}	GL78	$6.0 \ 10^{-24}$	$1.3 \ 10^{-23}$
	our model	$6.4 \ 10^{-24}$	$5.3 \ 10^{-24}$
$n_H = 10^4$ cm^{-3}	GL78	$1.5 \ 10^{-23}$	$1.3 \ 10^{-23}$
	our model	$5.1 \ 10^{-24}$	$3.9 \ 10^{-24}$
$n_H = 10^5$ cm^{-3}	GL78	$8.0 \ 10^{-24}$	$3.8 \ 10^{-24}$
	our model	$2.6 \ 10^{-24}$	$1.8 \ 10^{-24}$

extensive calculations of cooling rates due to various interstellar molecules. To make a direct comparison between their results and ours and get rid of differents of molecular abundances between the two sets of calculations, we compare the cooling efficiency per molecule defined as the ratio $\Lambda(X)/n(X)$ where $\Lambda(X)$ is the cooling rate per unit volume of gas due to the species X. Cooling efficiencies of O_2 and CO computed at the center of molecular clouds of various densities by GL78 and in our model are listed in Table 7. Typically, our values are three times lower than those of GL78; this is due to different collisional rates, but also to different expressions of the escape probability of the cooling photons: GL78 used the LVG approximation while we assume a static cloud where photons emitted in line wings have a larger probability to escape the cloud than those in the line center.

4. Conclusion

Several projects are planned in the near future to detect rotational lines of O_2 using millimeter and submillimeter receivers embarked on satellites or stratospheric balloons: ODIN for the 119 and 487 GHz lines, SWAS for the 487 GHz line, PRONAOS-SMH for the 368 GHz line and PIROG 8 for the 425 GHz line.

As a theoretical preparation to these projects, we have used an interstellar cloud model to compute the abundance and rotational populations of O_2 in order to predict the intensities of its main rotational lines. The model, which assumes steady-state equilibrium, solves a coupled set of equations: 1) The chemical balance equation for 136 species, mainly the simplest C- and O-bearing compounds and their ^{13}C and ^{18}O substitutions, leading to the distribution of their fractional abundances throughout the cloud. 2) The statistical equilibrium equations leading to the rotational population of the molecules H_2, CO and O_2 and the fine structure population of C, C$^+$ and O. 3) The thermal balance equation with gives the gas temperature distribution. 4) The transfer equation for the UV photons giving the photo-destruction rates of the chemical species as a function of depth within the cloud. The cloud model has been adapted from the one developed by Warin et al. (1996) by including the first 24 rotational levels of O_2. Their population is computed by using recent calculations of the collisional rates O_2–He from which we estimated O_2-H_2 rates; we also computed the spectroscopic parameters (energy levels and line strenghts) necessary to obtain the radiative rates. The main conclusions of this work can be summarized as follow:

– With the standard C/O abundance ratio of 0.4, the abundance of molecular oxygen increases very sharply with cloud visual extinction, so as to be comparable to that of CO, with O_2/CO ranging for 0.25 to 0.4 as A_V increases from 10 to 30, whatever the temperature and the hydrogen density. It must be noted that, even in the densest and most opaque clouds computed here, atomic oxygen remains more abundant than O_2 and represents between 20 and 30 % of the available gas phase oxygen.
– With the sensitivities expected for the receivers of the forthcoming missions, the detection of interstellar O_2 will be limited to dark clouds, with a possible exception for the ODIN receiver which could observe the 119 GHz line in

Table 8. Analytic fit of the O$_2$–He collision de-excitation rate (in cm^{3}s^{-1}): $k_{ul} = a_0 T^{0.3}$

(N_u, J_u)	(N_l, J_l)	a_0	(N_u, J_u)	(N_l, J_l)	a_0	(N_u, J_u)	(N_l, J_l)	a_0
(1, 1)	(1, 2)	1.1(-11)	(7, 6)	(3, 2)	4.0(-12)	(9, 10)	(7, 8)	1.7(-11)
	(1, 0)	2.4(-12)		(3, 3)	1.1(-12)	(11, 10)	(7, 6)	9.0(-12)
(3, 2)	(1, 1)	4.0(-12)		(3, 4)	1.8(-13)		(9, 8)	1.8(-11)
	(1, 2)	4.0(-12)		(5, 4)	1.4(-11)		(9, 9)	2.9(-13)
	(1, 0)	3.8(-12)		(5, 5)	1.7(-12)	(11, 11)	(7, 7)	6.4(-12)
(3, 3)	(1, 1)	6.8(-12)	(7, 7)	(1, 1)	5.4(-13)		(9, 8)	4.8(-13)
	(1, 2)	4.8(-12)		(1, 2)	4.4(-13)		(9, 9)	1.7(-11)
	(3, 2)	3.0(-12)		(3, 2)	2.8(-13)		(9, 10)	9.0(-13)
	(3, 4)	4.5(-12)		(3, 3)	4.0(-12)		(11, 10)	4.6(-12)
(3, 4)	(1, 1)	1.6(-12)		(3, 4)	1.0(-12)		(11, 12)	5.0(-12)
	(1, 2)	9.2(-12)		(5, 4)	7.9(-13)	(11, 12)	(5, 6)	8.7(-13)
	(1, 0)	9.4(-13)		(5, 5)	1.4(-11)		(7, 8)	6.8(-12)
	(3, 2)	1.5(-12)		(5, 6)	1.5(-12)		(9, 10)	1.8(-11)
(5, 4)	(1, 1)	2.0(-12)		(7, 6)	4.6(-12)	(13, 12)	(9, 8)	1.2(-11)
	(1, 2)	1.7(-12)		(7, 8)	5.0(-12)		(11, 10)	2.00(-11)
	(1, 0)	1.5(-12)	(7, 8)	(1, 1)	6.5(-14)	(13, 13)	(9, 9)	7.6(-12)
	(3, 2)	1.2(-11)		(1, 2)	8.7(-13)		(11, 10)	3.2(-13)
	(3, 3)	3.8(-12)		(1, 0)	3.9(-14)		(11, 11)	1.8(-11)
	(3, 4)	1.0(-12)		(3, 2)	4.8(-14)		(11, 12)	7.0(-13)
(5, 5)	(1, 1)	2.8(-12)		(3, 3)	2.7(-13)		(13, 12)	4.6(-12)
	(1, 2)	2.1(-12)		(3, 4)	5.0(-12)		(13, 14)	5.0(-12)
	(3, 2)	1.7(-12)		(5, 5)	7.5(-13)	(13, 14)	(7, 8)	8.7(-13)
	(3, 3)	1.2(-11)		(5, 6)	1.5(-11)		(9, 10)	7.7(-12)
	(3, 4)	3.2(-12)	(9, 8)	(5, 4)	6.5(-12)		(11, 12)	2.0(-11)
	(5, 4)	4.6(-12)		(5, 5)	2.0(-13)	(15, 14)	(11, 10)	1.4(-11)
	(5, 6)	5.0(-12)		(7, 6)	1.6(-11)		(13, 12)	2.2(-11)
(5, 6)	(1, 1)	5.7(-13)		(7, 7)	1.1(-12)	(15, 15)	(11, 11)	8.8(-12)
	(1, 2)	4.1(-12)	(9, 9)	(5, 5)	5.2(-12)		(13, 12)	1.6(-13)
	(1, 0)	3.5(-13)		(7, 6)	6.4(-13)		(13, 13)	1.9(-11)
	(3, 2)	4.1(-13)		(7, 7)	1.6(-11)		(13, 14)	5.0(-13)
	(3, 3)	1.5(-12)		(7, 8)	1.1(-12)		(15, 14)	4.6(-12)
	(3, 4)	1.5(-11)		(9, 8)	4.6(-12)		(15, 16)	5.0(-12)
	(5, 4)	4.8(-13)		(9, 10)	5.0(-12)	(15, 16)	(9, 10)	8.7(-13)
(7, 6)	(1, 1)	4.1(-13)	(9, 10)	(3, 4)	8.7(-13)		(11, 12)	8.6(-12)
	(1, 2)	2.3(-13)		(5, 6)	5.9(-12)		(13, 14)	2.2(-11)
	(1, 0)	3.3(-13)		(7, 7)	4.4(-13)			

translucent clouds ($A_V \sim 5$) provided the temperature is less than 50 K.

– Unlike the overall abundance of O$_2$, its rotational population, and consequently the intensity of its rotational lines are fairly sensitive to the temperature. The 368 GHz receiver of PRONAOS and the 487 GHz receivers of ODIN and SWAS are able to detect O$_2$ in opaque clouds ($A_V \geq 10$) with temperatures $T \sim 25$–50 K, somewhat larger than usually expected in dark clouds. Due to larger line intensities, the PIROG 8 receiver could detect the 425 GHz line in less opaque clouds ($A_V \sim 6$–7) in the same range of temperatures.

– Because O$_2$ is rather easily photodissociated, the regions submitted to an intense UV radiation field are very unfavourable to the detection of O$_2$. Typically, if the external UV radiation field is enhanced by a factor 1000 with respect to the local standard value, only the ODIN receiver at 119 GHz is able to detect O$_2$ in dark clouds with $A_V \sim 10$,

while the three other lines will be observable in more opaque clouds ($A_V \sim 20$).

– The most drastic parameter that controls the abundance of O$_2$ (as well as that of OH and H$_2$O) and, consequently, the detectability of its rotational lines, is the C/O elemental abundance ratio in the gas phase. The molecule CO is so easily formed in interstellar clouds and so stable that its abundance is very rapidly limited by the available gas phase carbon or oxygen depending to wether C < O or C > O. As the carbon abundance increases and approches that of oxygen, the amount of oxygen available to produce oxygen-bearing molecules other than CO is considerably reduced. For typical dark cloud conditions, as C/O increases from the standard value of 0.4 to 2, O being fixed, the O$_2$ abundance drops by a factor $\sim 4 \ 10^4$; at the same time, the H$_2$O and OH abundances are also decreased, but to a lesser extent, by a factor 2500 and 30, respectively. If C/O$\sim$1, the 119 GHz line of O$_2$ appears accessible to the ODIN receiver only in

very opaque clouds ($A_V \sim 20$), the three other lines being unobservable as soon as the C/O ratio is larger than 0.7. Because of this strong sensitivity to C/O, the detection of O_2 could serve to constrain the carbon and oxygen abundances if parameters like density, temperature, UV field... could be derived by another way; it must be however noted that the amount of O_2 is very sensitive to other physical conditions such as the ionization degree, as indicated by alternative model calculations.

– In regions where the O_2 column densities are large enough to be detectable, the rate coefficient of the reaction $O+OH \rightarrow O_2+H$, the main route to O_2, has little influence on its abundance. It however controls the OH abundance since it is the main destruction process of this molecule. An experimental study of the $O+OH \rightarrow O_2+H$ reaction at low temperatures would be of great interest for this problem.

– Our model calculations also predict that radiative de-excitation of O_2 could be an important cooling agent of cold molecular gas, to be included in models. Under favourable conditions for the formation of O_2, its cooling efficiency is comparable to that of CO mainly because the lower line strenghts of the O_2 lines are compensated by their lower opacities.

Appendix A: the collisional rates O_2–He

See Table 8.

References

Adams N.G., Smith D., Alge E., 1984, J. Chem. Phys. 81, 1778

Adams N.G., Smith D., 1987, Astrochemistry, 120th IAU symposium, D. Reidel Publishing Company

Anicich V.G. 1993, J.Phys.Chem.Ref.Data 22, 1469

Anders E., Grevesse N., 1989, Geochimica et Cosmochimica Acta 53, 197

Beaudin et al., 1994, 24th European Microwave Conference proceeding Vol III, 1955

Bergman P., 1995, ApJ 445, 167

Black J. H., Smith P. L., 1984, ApJ 277, 562

Boissé P., 1990, A&A 228, 483

Cheung A.S.-C., Mok D.K.-W., Jamieson M.J. et al., 1993, J.Chem.Phys. 99, 1086

Chieze J.P., Pineau des Forêts G., 1989, A&A 221, 89

Combes F., Wiklind T., 1995, A&A 303, L61

Corey G. C., 1984, J. Chem. Phys. 81, 2678

Corey G. C., Alexander M. H., Schaefer J., 1986, J. Chem. Phys. 85, 2726

Davidsson J., Stenholm L.G., 1990, A&A 230, 504

Ehrenfreund P., Breukers R., d'Hendecourt L., Greenberg J.M., 1992, A&A 260, 431

Gies H.P.F., Gibson S.T., McCoy D.G. et al., 1981, JQSRT 26, 469

Goldsmith P. F., Langer W. D., 1978, ApJ 222, 881

Gordy W., Cook R. L., 1984, Microvawe molecular spectra, Wiley Interscience Publication

Herbst E., Klemperer W. 1973, ApJ 185, 505

Herzberg G., 1950, Molecular spectra and molecular structure: I- Spectra of diatomic molecules, Van Nostrand Reinhold Company

Howard M.J., Smith I.W.M. 1980, J.Chem.Soc.Faraday Trans. 277, 997

Hudson R. D., 1971, Rev. Geophys. Space Phys. 9, 305

Kirby K., Constantinides E. R., Babeu S., Oppenheimer M., Victor G. A., 1979, At. Data Nucl. Tables 22, 63

Langer W.D., Graedel T.E., 1989. ApJS 69, 241

Le Bourlot J., Pineau des Forêts G., Roueff E., 1995, A&A 297, 251

Mathis N., Mezger P. G., Panagia J. J., 1983, A&A 128, 212

Millar T.J., Farquhar P.R.A., Willacy K. 1996, in press in A&AS

Orlikowsky T., 1986, Molecular Physics 56, 35

Savage B.D., Sembach K.R., 1996, ARA&A 34, 279

Spaans M., 1996, A&A 307, 271

Tinkham M., Strandberg M. W. P., 1955, Phys. Rev. 97, 937

Viala Y.P. 1986, A&AS 64, 391

Viala Y.P., Walmsley C.M. 1976, A&A 50, 1

Warin S., Benayoun J. J., Viala Y. P., 1996, A&A 308, 535

Yoshino K., Freeman D.E., Esmond J.R., Parkinson W.H., 1983, Plant. Space Sci. 31, 339